JOURNAL OF SOLID STATE CHEMISTRY 95, 99–110 (1991)

On the Mechanism of Solvolytic Decompositions of Mixed Halides

GUO LIU AND H. A. EICK*

Department of Chemistry, Michigan State University, East Lansing, Michigan 48824-1322

Received February 12, 1991; in revised form June 19, 1991

Synthesis of the phase-pure mixed-valent europium chlorides, Eu_4Cl_9, Eu_5Cl_{11}, and $Eu_{14}Cl_{33}$, is reported. X-ray powder diffraction data are presented for $NdBr_3 \cdot (THF)_4$. The structures of metastable dihalides synthesized by solvolytic decomposition, fluorite-type $LnCl_2$, Ln = Sm, Eu, and anti-Fe_2P-type BaX_2, X = Cl, Br, and that of the cluster-type mixed-valent halide precursor, are described in terms of close-packed layers and a solvolytic decomposition mechanism is proposed. In this mechanism the Ln^{3+} ions at the solvent–solid interface are removed as LnX_3 (solvate) from atomic planes perpendicular to the three-fold inversion axis of the precursor and remaining LnX_2 ions relax immediately; primarily in-layer cation rearrangements lead to the fluorite-type structure upon subsequent layer collapse, whereas both in-layer and out-of-layer cation displacements yield the anti-Fe_2P-type structure.

Introduction

Solvolytic decomposition is a liquid–solid reaction in which selected ions at the liquid–solid interface are solvated. For example, insoluble $PrO_2(s)$ can be prepared by selectively dissolving the Pr^{3+} ions from "Pr_6O_{11}" with acetic acid (*1*). We have reported previously that low temperature solvolytic decomposition reactions of mixed halide precursors with fluorite-related superstructures yield the metastable fluorite (high temperature) form of $LnCl_2$ (Ln = Sm, Eu) (*2*) and the anti-Fe_2P (high pressure) form of BaX_2 (X = Cl, Br) (*3*). Thermodynamic and kinetic considerations suggest these apparently kinetically controlled reactions are topochemical. It is indeed surprising that solvolytic decompositions of isostructural cluster-type $Ln_{14}Cl_{33}$ and $Ba_9Ln_5Br_{33}$ produce, respectively, metastable fluorite-type $LnCl_2$ and (hexagonal) anti-Fe_2P-type $BaBr_2$. The decomposition products of these low temperature reactions have symmetries higher than those of both their precursor (parent) phases and the normal modifications, suggesting that symmetry factors play a significant role in the reaction mechanisms. In this paper we detail the structural relationships among the precursor phases and the solvolytic decomposition products through layer analysis and propose a mechanism consistent with the topochemical nature of these solvolytic decomposition reactions.

Experimental

Since specific details of precursor synthesis and solvolytic decomposition (extraction

* To whom correspondence should be addressed.

0022-4596/91 $3.00

or leaching) have been described previously (*2, 3*), only general comments will be given here. All sample manipulations were effected in a glovebox whose recirculated Ar atmosphere was continuously purged of both oxygen (BASF catalyst) and moisture (molecular sieves). Typical glovebox moisture content during sample manipulation was 10 ppm_v. Solvolytic decomposition reactions were effected in an all-glass extraction apparatus with a Soxhlet extractor fitted with Teflon stopcocks and Teflon joint sleeves. Dehydrated and deoxygenated tetrahydrofuran (THF) was transferred under high vacuum to the reflux flask and the extractor with the sample in a removable thimble was transferred under Ar from the glovebox to the extraction apparatus. Extraction was effected in a dry argon atmosphere and the extracted product was blanketed with Ar during transfer to the glove box. Phase purity was always established by Guinier X-ray powder diffraction analysis.

Precursor Synthesis

The mixed halide, $Sm_9Gd_5Cl_{33}$, was synthesized in 0.5- to 1.0-g quantities either by hydrogen reduction of a $SmCl_3$–$GdCl_3$ mixture as described previously (*2*) or by the ceramic method from an intimately ground 1 : 1 molar mixture of $SmCl_2$ and $GdCl_3$. In the latter procedure the specimen was sealed into an outgassed quartz tube under vacuum, heated at 500°C for 4 days and then cooled slowly. The brown, pulverized product contained unreacted $GdCl_3$. In this and previously reported preparations (*2, 3*) the mixed halides or mixed-valent halides were obtained as mixtures with excess lanthanoid trihalide.

We developed procedures for synthesis of phase-pure, 0.5- to 1.0-g samples of the mixed-valent europium chloride precursor phases, Eu_4Cl_9, Eu_5Cl_{11}, and $Eu_{14}Cl_{33}$:

Eu_4Cl_9. An intimately ground 3 : 1 molar mixture of $EuCl_2$: $EuCl_3$ was sealed into an outgassed quartz tube under vacuum and heated at 500°C for 5 days, then quenched.

Eu_5Cl_{11}. Two procedures were used: thermal decomposition and hydrogen reduction. An $EuCl_3$ specimen heated at 500°C for 5 hr in a 0.1- to 0.01-Torr vacuum yield the blue product. It was also prepared by reducing $EuCl_3$ with H_2 at 400°C for 2 days.

$Eu_{14}Cl_{33}$. Two procedures were used: thermal decomposition and solid state reaction. $EuCl_3$ heated in vacuum at 440°C for 12 hr was converted to the black $Eu_{14}Cl_{33}$. The compound was also prepared from a 3 : 2 molar mixture of $EuCl_2$: $EuCl_3$ sealed in quartz under vacuum, heated at 500°C for 5 days, and then quenched.

To check for intermediate products during solvolytic decomposition the reaction was stopped at regular intervals. The solvent was removed, the residue in the Soxhlet extractor evacuated to dryness, and the remaining solids examined by both X-ray powder diffraction and solid state IR spectroscopy. The THF complexes present in the extractor thimble can be synthesized as pure phases by contacting anhydrous $NdBr_3$ or $EuCl_3$ with THF and then evacuating the product to dryness. Their compositions were determined from the weight loss a specimen experienced when it was heated at 130°C for many hours in a high vacuum.

Results and Discussion

Solvolytic Decompositions

The metastable halides produced by solvolytic decomposition are well-crystallized; they produce moderately sharp X-ray powder diffraction reflections. The lattice parameters of metastable BaX_2 (X = Cl, Br) show a systematic relationship with the precursor (*3*); those of $LnCl_2$ are precursor independent. Thermal tests have demonstrated the kinetically controlled nature of solvolytic decomposition (*2*).

In previous studies (*3*) we observed a

crystalline intermediate when $Ba_9Ln_5Br_{33}$ (Ln = La, Nd) precursors were examined after 30 min of THF extraction. Subsequent experiments revealed similar behavior in other systems. These intermediates are actually $LnX_3 \cdot$ THF complexes; in the neodymium case the formula of the complex is $NdBr_3 \cdot (THF)_4$ (*3*). The normal orthorhombic modification of $NdBr_3$ results when THF is removed from $NdBr_3 \cdot (THF)_4$. When a 1- to 3-g specimen of $Ba_9Ln_5Br_{33}$ precursor that contained excess $LnBr_3$ was subjected to THF extraction, the $NdBr_3 \cdot (THF)_4$ complex was observable in the X-ray powder diffraction patterns after 3 hr of extraction. The powder diffraction pattern of this complex was indexed on triclinic symmetry by the program TREOR (*4*) with a figure-of-merit, $M(20) = 26$ (*5*); Miller indices, observed intensities, and observed and calculated interplanar d-spacings are presented in Table I.

The $EuCl_3 \cdot (THF)_n$ ($1 < n < 2$) complex that formed after 30 min THF extraction of $EuCl_{2+x}$ specimens that contained a trace of $EuCl_3$ also had an X-ray powder diffraction pattern similar to that formed between pure $EuCl_3$ and THF. After 6 hr of extraction this THF complex could no longer be detected by X-ray diffraction. With pure precursors such as Eu_4Cl_9 the complex was not observable by X-ray diffraction after 30 min extraction. However, a trace of the THF complex could be detected in the solid state FTIR spectra of these specimens after 5 hr of extraction. After an additional 10 hr of extraction the THF complex was no longer visible in the IR spectrum. The same fluorite-type $EuCl_2$ was obtained irrespective of the mixed-valent europium chloride specimen extracted. The absence of this THF complex confirms that all Eu^{3+} cations (and associated chloride anions) were extracted from the precursor. In other words, regardless of the overall oxidation state of the Eu atoms in the precursor, only Eu^{2+} ions remain in the extraction product.

X-ray powder diffraction data and specimen color changes verified that the mixed-valent chlorides, $LnCl_{2+x}$ (Ln = Sm, Eu), are decomposed quickly by THF. Upon leaching the color of $EuCl_{2+x}$ changes almost instantly from blue or black to white. The $Ba_9Ln_5Br_{33}$ precursors were also decomposed quickly, but less rapidly than the $LnCl_{2+x}$ specimens. On the other hand, extraction of $BaCl_2$–$LnCl_3$ precursors proceeded slowly. While no trace of the $EuCl_{2+x}$ precursor could be found (by X-ray analysis) after 30 min extraction, the $Ba_{17}Sm_{10}Cl_{64}$ precursor was apparent even after 5–6 days of extraction. No additional phase was observed in any of the systems examined.

Oxidehalide contamination appears to hinder solvolytic decomposition. The cluster-type $Ln_{14}X_{32}O$ oxidehalide and $Ln_{14}X_{33}$ halide have structures essentially indistinguishable by X-ray diffraction. From an analysis of the Kapustinskii equation (*6*) it is apparent that oxidehalide lattice energies must be greater than those of pure halides or mixed halides. In the $Ln_{14}X_{32}O$ structure oxygen atoms occupy the cluster centers (*7*) where the structure must undergo significant changes upon solvolytic decomposition. Therefore the $M_8Ln_6X_{32}O$ ($M = Ln'^{2+}$ or Ba^{2+}) structure is probably too stable for THF to decompose. The inability of THF to extract completely "$Sm_9Gd_5Cl_{33}$" precursors prepared by the ceramic method suggests the presence of a $Sm_8Gd_6Cl_{32}O$ impurity; it could result from reaction with the quartz container.

These considerations suggest that the mixed-valent halide synthesis procedure must preclude oxidehalide formation. Oxygen- and water-free handling and storage conditions are essential. Low decomposition temperatures and short heating times would also tend to minimize oxidehalide contamination. For the europium mixed-valent chlorides the various synthesis methods used, partial reduction with hydrogen, ther-

TABLE I

MILLER INDICES, OBSERVED (GUINIER) INTENSITIES, AND OBSERVED AND CALCULATED INTERPLANAR *d*-SPACINGS FOR TRICLINIC $NdBr_3 \cdot (THF)_4$

a = 8.352(1) Å, b = 15.915(3) Å, c = 9.429(1) Å
α = 100.02(2)°, β = 105.26(2)°, and γ = 87.54(2)°

h	k	l	d_c(Å)	d_o(Å)	I_o	h	k	l	d_c(Å)	d_o(Å)	I_o
0	1	0	15.672	15.696	vw^+	1	−2	2	3.4074	3.4058	w^-
0	0	1	8.9660	8.9626	s	−2	−3	1	3.3449	3.3476	vw
0	−1	1	8.4190	8.4083	s	−2	−2	2	3.3435		
1	0	0	8.0578	8.0438	vs	−2	3	1	3.1126	3.1121	vw^+
0	2	0	7.8362	7.8352	vs	−2	−3	2	3.0846	3.0843	vw
0	1	1	7.2714	7.2727	m	1	2	2	3.0781		
−1	1	0	7.1750	7.1675	vw^+	−1	0	3	3.0748	3.0750	vw
1	1	0	7.1573			−2	2	2	3.0389		
−1	0	1	6.9595	6.9579	w^+	0	−1	3	3.0314	3.0332	vw^+
−1	−1	1	6.6870	6.6894	w^+	−1	−5	1	3.0062	3.0074	vw^+
0	−2	1	6.4658	6.4666	w	0	0	3	2.9887	2.9883	w
−1	1	1	6.0777	6.0732	m^-	0	−2	3	2.9640	2.9651	vw
−1	2	0	5.6263			−2	−4	1	2.9415	2.9409	w
1	2	0	5.6092	5.6123	s	0	1	3	2.8486	2.8463	w
−1	−2	1	5.5708	5.5704	vw^+	0	5	1	2.8146		
0	3	0	5.2241			−2	4	0	2.8132	2.8129	w
1	−1	1	5.2230	5.2230	w^+	0	−3	3	2.8063	2.8060	vw
1	1	1	4.9054			2	4	0	2.8046		
−1	2	1	4.9006	4.9020	w^+	−1	−5	2	2.7867	2.7878	vw
0	−3	1	4.8869			−2	−4	2	2.7854		
1	−2	1	4.6414	4.6448	w	−2	−2	3	2.7477	2.7484	vw^+
0	−1	2	4.5164	4.5166	w	2	3	1	2.7464		
0	0	2	4.4830	4.4851	vw^-	−2	3	2	2.7384	2.7382	vw
−1	−1	2	4.4684	4.4662	vw^-	−1	2	3	2.7079	2.7085	vw
−1	−3	1	4.4621			−3	−2	1	2.6609	2.6610	w^-
1	2	1	4.2174	4.2175	w^+	−3	1	0	2.6487	2.6492	vw
0	3	1	4.2149			0	2	3	2.6476		
−1	−2	2	4.1688	4.1707	vw	−2	−3	3	2.6198	2.6197	vw^+
0	1	2	4.1298	4.1306	vw	1	−1	3	2.6193		
−1	−1	2	4.0962			1	0	3	2.5911	2.5912	vw^+
−2	0	1	4.0942	4.0941	m^-	1	5	1	2.5900		
1	−3	1	3.9428			2	1	2	2.5896		
−1	3	1	3.9421	3.9414	m^+	−3	2	1	2.5797		
−2	1	0	3.9049			1	−2	3	2.5759	2.5768	vw
2	1	0	3.8992	3.9048	vw	−1	−6	1	2.5558	2.5556	vw^+
−2	1	1	3.8915	3.8930	vw	3	2	0	2.5384	2.5392	vw
0	−4	1	3.8357	3.8369	vw^+	−2	−5	2	2.4936		
−2	−2	1	3.7442	3.7441	vw	−2	2	3	2.4930	2.4929	vw
−1	−3	2	3.6976	3.6976	vw	2	−3	2	2.4839		
−1	−4	1	3.6186			1	6	0	2.4826	2.4830	w
−1	2	2	3.6139	3.6151	w^-	2	4	1	2.4725		
−2	2	0	3.5875	3.5865	w	1	−3	3	2.4707	2.4712	w^-
1	−1	2	3.5631	3.5619	w	−3	−3	2	2.4407	2.4405	vw
−2	2	1	3.5234			−3	2	2	2.4196	2.4203	w
1	4	0	3.5194	3.5212	w	−1	−5	3	2.4129	2.4119	w

mal decomposition, and even solid state reactions between $EuCl_2$ and $EuCl_3$, produced pure compounds that could be decomposed completely by THF. For the samarium mixed chlorides, hydrogen reduction of the $SmCl_3$: $GdCl_3$ 1 : 1 mixture yielded the more readily extracted specimens. The barium mixed bromides were not obviously subject to oxygen contamination, but $BaCl_2$ is known to attack quartz at high temperatures (*8*). The barium chloride precursors, especially the $BaCl_2$–$LaCl_3$ mixtures that required reaction temperatures above 800°C, may have contained oxidechloride since complete extraction could not be achieved. Consistent with basicity trends, $Ba_{17}Sm_{10}Cl_{64}$ is a better precursor than "Ba_2LaCl_7."

The Reaction Mechanism

Although additional experiments (e.g., electron diffraction analysis) are required to confirm chemical and structural changes at the microscopic level, the various macroscopic observations allow a mechanism to be postulated.

A dissolution–reprecipitation mechanism like that postulated for the formation of γ-MnO_2(s) from Mn_3O_4 leached by a mineral acid such as dilute HCl (*9*) is unlikely for organic solvents. In dilute HCl the Mn_3O_4 dissolves into Mn^{2+} and Mn^{3+} ions with the latter disproportionating into Mn^{2+} and γ-MnO_2(s). The oxides of both the Mn^{2+} and the Mn^{3+} ions are soluble in the acid. In the mixed halide decomposition the trihalide is soluble in the organic solvent, but the dihalide is not. When $SmCl_3 \cdot (THF)_n$ is reduced in THF, the $SmCl_2$ precipitate is the normal (red) $PbCl_2$-type (*10*) and not the metastable (blue) CaF_2-type modification. Furthermore, a dissolution–reprecipitation mechanism should not produce the highly crystalline precipitate observed in this work because rapid precipitation at low temperatures precludes annealing. Nor in a dissolution–reprecipitation mechanism should the unit cell dimension(s) of the metastable product vary systematically with the mixed halide precursor as do those of metastable BaX_2 (*3*).

A combined dissolution–electron transfer mechanism like that postulated for the solvolytic decomposition of Pb_3O_4 in dilute nitric acid (*11*), while possible for $LnCl_{2+x}$ (Ln = Eu, Sm) precursors, can also be ruled out. The reaction products do not change when the Eu^{3+} or Sm^{3+} ions are replaced by La^{3+} or Gd^{3+}, neither of which can undergo reduction.

Therefore, the solvolytic decomposition of mixed halides must involve selective dissolution of the trivalent cations (and associated anions), and the metastable dihalides that result must be the collapsed, reorganized product of these insoluble cations and associated anions. Thus the structures of the metastable forms and those of the precursors should be closely related and their relationships should be explainable in topochemical terms. THF decompositions of the fluorite-related vernier-type mixed-valent chlorides Eu_nCl_{2n+1} (n = 4, 5) lead to fluorite-type $EuCl_2$ in a relatively straightforward topochemical reaction and are not discussed here. Solvolytic decompositions of the cluster-type mixed halides, on the other hand, are of special interest because for Ln^{2+} (Ln = Sm, Eu) and Ba^{2+} ions isostructural precursors yield metastable dihalides with different structures.

Solvolytic decomposition is a typical solid–liquid reaction and is anisotropic because some lattice planes have higher reactivities than others. In solvolytic decompositions the element of highest symmetry in the cluster-type precursor, the three-fold inversion axis, is retained in both the cubic fluorite-type $LnCl_2$ and the hexagonal anti-Fe_2P-type BaX_2 modifications. This retention suggests that the planes perpendicular to this axis are the solvolytic decomposition frontiers.

Structures of Related Halide Compounds

To facilitate discussion of the proposed topochemical changes, the relevant structures are described briefly in terms of atomic close-packed layers perpendicular to the threefold axis.

1. The fluorite-type structure. This face-centered cubic structure is commonly described in terms of hexagonally close-packed layers of cations normal to the threefold axis and stacked in the sequence ABCABC. . . . The anions occupy all the tetrahedral holes and form separate hexagonal close-packed layers parallel to the cation layers. To facilitate comparison with the other structures which are either hexagonal or rhombohedral, the fluorite structure was transformed to an hexagonal setting (with no loss of symmetry). The transformation used was: $\mathbf{a}_h = \mathbf{a}_c - \mathbf{c}_c$, $\mathbf{b}_h = -\mathbf{a}_c + \mathbf{b}_c$, and $\mathbf{c}_h = \mathbf{a}_c + \mathbf{b}_c + \mathbf{c}_c$.

2. The $PbCl_2$-type structure. The normal modifications of $LnCl_2$ (Ln = Nd, Sm, Eu) and BaX_2 (X = Cl, Br, I), along with many other AB_2-type compounds, exhibit this orthorhombic structure. The structure of $EuCl_2$, which was refined by Bärnighausen (*12*) in space group 62, *Pbnm*, can be thought of as a considerably distorted close-packing of the halogen atoms with the cations accommodated in the same plane. The layers are stacked in an ABAB . . . (double layer) fashion. The cation arrangement in this structure can be derived from a single hexagonally close-packed layer as depicted in Fig. 1a. Exactly half of the cations are displaced from the layer by $c/2$ such that the sixfold axes are destroyed while zigzag cation–cation chains are formed in each layer and inversion centers are created between any two adjacent layers.

3. The anti-Fe_2P-type structure. Anti-Fe_2P-type BaI_2 was prepared under high pressure and the structure was refined with single crystal data (*13*). This hexagonal structure, space group 189, $P\bar{6}2m$, exhibits close-packing similar to that of the $PbCl_2$-type structure. The cation positions in this two-layer structure can also be derived from hexagonal close-packing as shown in Fig. 1b. The cation arrangement of the anti-Fe_2P-type structure results when $\frac{1}{3}$ of the metal atoms are displaced from a hexagonal close-packed layer by $c/2$ such that a sixfold inversion axis remains.

The atoms in the anti-Fe_2P-type structure are slightly more densely packed (0.8% higher packing efficiency for BaI_2 (*13*)) than those in the $PbCl_2$-type structure. Therefore, there is a slight increase in effective coordination numbers in the former structure.

4. The fluorite-related superstructure of cluster-type $M_9^{2+}Ln_5^{3+}Cl_{33}$. The structure of oxygen-containing $Nd_{14}Cl_{32}O$ was solved by single crystal techniques (*7*) and subsequently that of $Nd_{14}Cl_{33}$ was solved with a triply twinned crystal (*14*). The true symmetry of $Nd_{14}Cl_{33}$ is triclinic, but it can be approximated in a rhombohedral setting (space group 148, $R\bar{3}$). One unit cell contains 27 $NdCl_2$ and 15 $NdCl_3$ units (three formula units), and contains 3 Nd_6Cl_{37} ($Nd_1^{2+}Nd_5^{3+}Cl_{37}$) clusters in which the six cations are situated in an octahedral arrangement (*14*).

Clustering of the trivalent cations in the superstructure is apparently caused by the "extra" anions that accompany the Ln^{3+} ions. Eitel (*14*) and Bevan and co-workers (*15, 16*) have described the formation of clusters from the fluorite coordination polyhedra. From the viewpoint of atomic close-packing, a projection down the threefold axis can illustrate the fluorite-related features of this superstructure better than any other illustration. A single cation layer of $Ln_{14}Cl_{33}$ is shown in Fig. 1c; the trivalent cations are ordered along threefold axes in each layer. (In the $M_{14}Cl_{33}$ structure one of the six clustered atoms must be divalent; that distinction is not apparent in this rhombohedral projection.) Cluster formation oc-

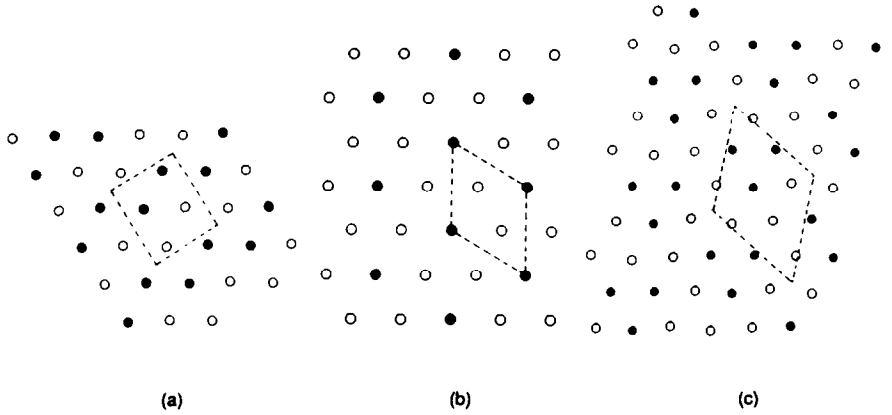

FIG. 1. The cation arrangement in various structures illustrating their derivations from hexagonally close-packed layers. (a) The $PbCl_2$-type double (solid and open circle) layer structure; (b) the anti-Fe_2P-type double (solid and open circle) layer structure; (c) a typical layer of the cluster-type $Ln_{14}X_{33}$ structure. In (c) the open circles represent Ln^{2+} and the solid circles Ln^{3+} ions.

curs between two adjacent cation layers as shown in Fig. 2. The rhombohedral supercell corresponds to six cation layers in comparison to the three cation layers (. . . ABC . . .) in the fluorite structure. The

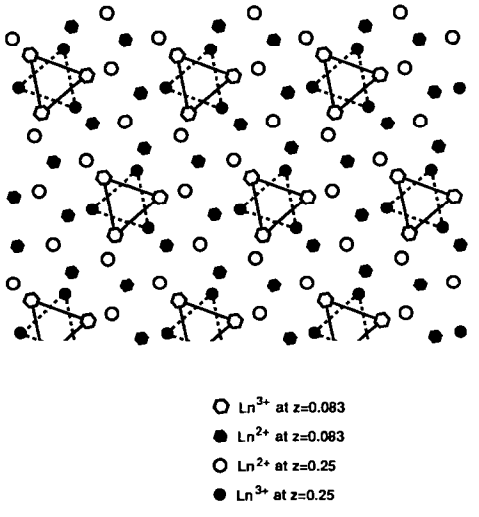

FIG. 2. Two adjacent cation layers in the $M_{14}X_{33}$ structure illustrating the M_6X_{37} clusters. If X represents only a monovalent anion, one of the six cluster cations (here labeled Ln^{3+}) must be divalent.

layer stackings of the cluster-type structure, together with those of the other structure types described above, are illustrated in Fig. 3. In Fig. 3a the cations and anions are not shown exactly at the ideal z positions; displacements are 0.02–0.5 Å from the indicated positions. This figure demonstrates that the principal differences between the fluorite- and the cluster-type layer stackings are the "extra" anion layers in this superstructure.

The $Ln_{14}Cl_{33}$ to Fluorite-Type $LnCl_2$ (Ln = Sm, Eu) Transformation

In a solvolytic decomposition the trivalent cations and accompanying anions are removed selectively from the mixed-valent halide lattice. Thus the clusters can be regarded as the decomposition centers. Were the trivalent cations and associated anions removed so gently from the layers (Fig. 4a) at low temperatures that the remainder of the lattice is perturbed only slightly, a transitory intermediate (LnX_2) lattice (Fig. 4b) comprised of Ln^{2+} and Cl^- layers with a large number of vacancies would result. If the cations in this highly unstable intermedi-

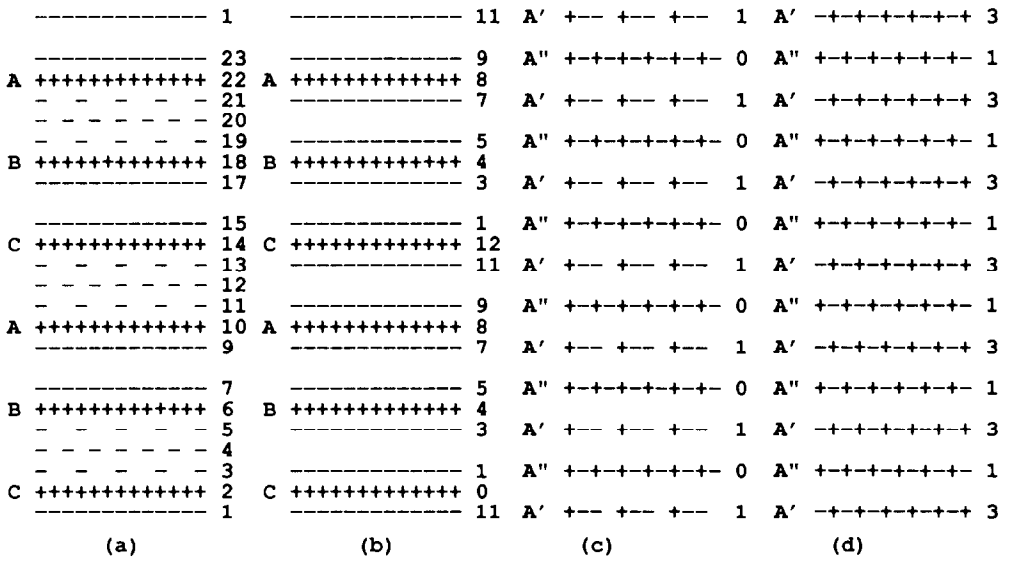

FIG. 3. Schematic illustration of layer stackings of various structure types. Numbers adjacent to layers represent z coordinates. + + + +, cation layer; -----, anion layer; +--, +-+-+-, or -+-+-+, cations and anions in the same layer. (a) $Ln_{14}X_{33}$ cluster type; z coordinates in 24th. (b) Fluorite-type in hexagonal setting; z coordinates in 12th. (c) Anti-Fe_2P-type; z coordinates in halves. Note that the number of cations in the A′ layers is half that in the A″ layers. (d) $PbCl_2$-type; z coordinates in fourths. The packings of A′ and A″ are identical but the stacking order is different. Structures (a), (b), and (d) are centrosymmetric; (c) is not. The $BaCl_2$ anion–anion and the A′–A″ layer spacings in the different structure types are: (b) 2.111 Å, (c) 2.308 Å, and (d) 2.366 Å.

ate lattice rearranged to eliminate the vacancies with primarily *in-layer* displacements, i.e., movement only perpendicular to the threefold axis, each resulting layer would become hexagonally close-packed (Fig. 4c). Retention of the stacking sequence (ABCABC. . .) upon collapse of the anion layers should yield with minimal adjustment the observed fluorite-type structure. This interlayer structural change can be understood by noting the similarity of the layer stackings in Figs. 3a and 3b. Furthermore, as the exterior portion of any crystallite transforms to the fluorite-type structure, voids produced upon structural collapse can allow solvent to diffuse into and away from the reaction frontier.

Even though direct observation of this microscopic process has not been possible, we believe it to be the most likely mechanism for two reasons. First, such a change would approximate a one-step process. The intermediate could be neither trapped nor observed, consistent with experimental observations that no trace of any new phase is seen by X-ray diffraction. Second, such an in-layer ion rearrangement with subsequent layer collapse involves minimal structural change and should have a low activation energy, consistent with the observation that decompositions which yield fluorite-type phases proceed exceedingly rapidly.

Based on the above discussions, the cubic lattice parameter, a_c, of $LnCl_2$ can be related to the $Ln_{14}Cl_{33}$ hexagonal (supercell) lattice parameters, a_h (super) and c_h (super). In Fig. 5 the relation between a_h (super) and a_c in a cation layer is illustrated. From the assumed hexagonal cell geometry displayed in Fig. 5 we find $\sqrt{2} \cdot a_c/a_h$ (super) = 0.756, or a_c =

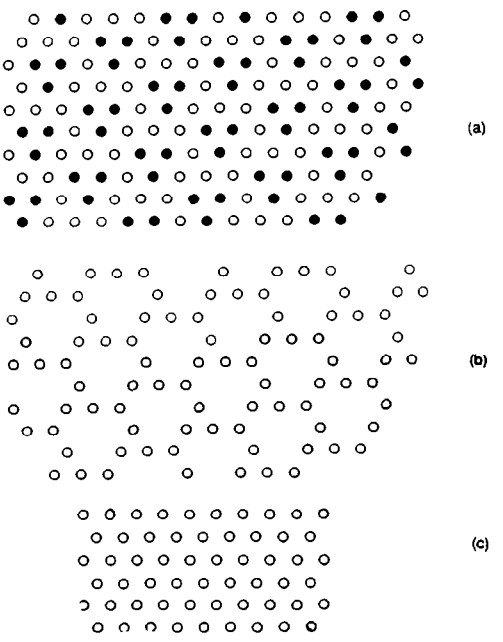

FIG. 4. Proposed structural changes during solvolytic decomposition in a single cation layer of $Ln_{14}Cl_{33}$. (solid circles, Ln^{3+}; open circles, Ln^{2+}) (a) Before extraction, (b) hypothetical intermediate, (c) reorganized structure.

$0.534 \cdot a_h$(super). From our previous descriptions we know that c_h(super) is parallel to the cubic body diagonal ($= \sqrt{3} \cdot a_c$) and the supercell is six-layered while the cubic cell is three-layered. Thus we have $(6/3)\sqrt{3} \cdot a_c = c_h$ (super), that is, $a_c = (\sqrt{3}/6) \cdot c_h(\text{super}) = 0.2887 \cdot c_h(\text{super})$. The cubic lattice parameters derived from both a_h(super) and c_h(super), together with observed values, are listed in Table II. The proximity between derived and observed parameters is considered support for the proposed mechanism.

The $Ba_9Ln_5Br_{33}$ (Ln = La, Nd) to Anti-Fe_2P-Type $BaBr_2$ Transformation

$Ba_9Ln_5Br_{33}$ exhibits the cluster-type ($Ln_{14}Cl_{33}$) structure; the $Ba_{17}Ln_{10}Cl_{64}$ structure has not been solved, but is fluorite-related (*17*). Every barium-containing mixed halide upon solvolytic decomposition yielded the anti-Fe_2P-type structure even though a fluorite-type (high-temperature) modification of $BaCl_2$ can be quenched (*18*). No trace of fluorite-type $BaCl_2$ or $BaBr_2$ was observed in any solvolytic decomposition experiment. These results suggest that solvolytic decompositions of the barium-related mixed halides proceed by a reaction mechanism different from that for lanthanoid mixed-valent chlorides.

The major difference between BaX_2 and LnX_2 is their cationic radii. The CN VIII ionic radius of Ba^{2+} (1.56 Å) is ~10% larger than those of Sm^{2+} (1.41 Å) and Eu^{2+} (1.39 Å) (*19*). The data in Table III suggest the M^{2+}/Ln^{3+} radius ratio to be the major factor in determining product structure. When LnX_3 species are removed from the BaX_2–LnX_3 precursors the lattice collapses in a way different from that found in the $LnCl_{2+x}$ precursors, presumably because of the larger-sized Ba^{2+} ion. It has been shown previously that cation positions in the anti-Fe_2P-type structure can be derived through displacement of hexagonal close-packed layers. Formation of this phase upon solvolytic decomposition suggests that in-layer rearrangements of the cations to form hexagonal close-packed layers are energetically less favorable for BaX_2 than for LnX_2. Instead, both out-of-layer and in-layer displacements occur. These locally confined displacements lead to the mixing of the cations and anions in the same layers and to formation of the anti-Fe_2P-type structure as can be seen in Fig. 3c.

Metastable phases formed in this way are more dense than the normal forms, in contrast to the significantly less dense fluorite-type modifications. This result suggests for BaX_2 an internal pressure which may be created by the size incompatibility mentioned above, and is probably the cause of the out-of-layer displacements.

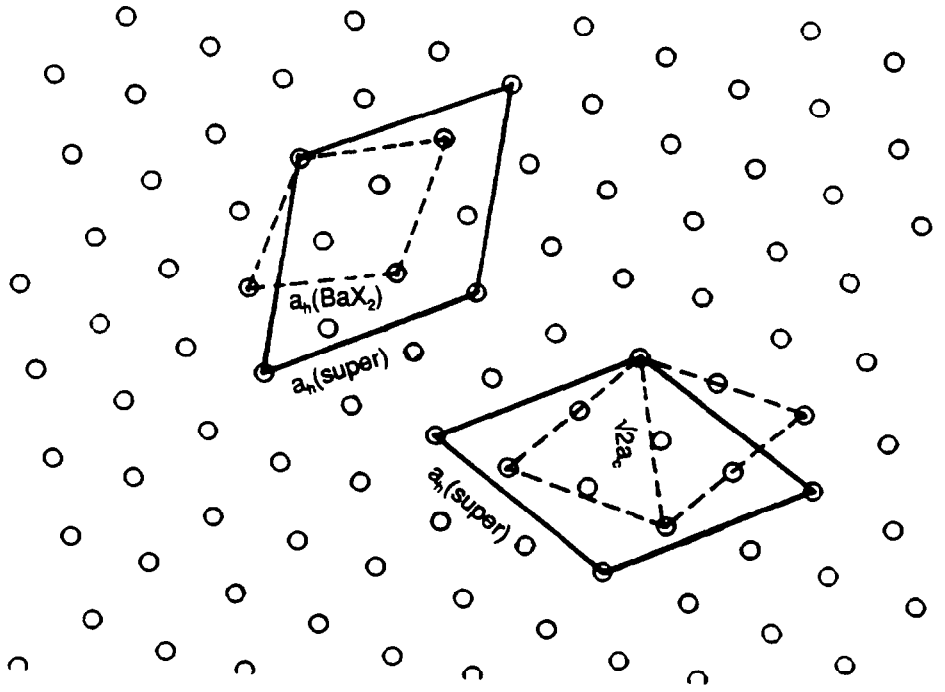

FIG. 5. Lattice parameter relationships between the $M_{14}X_{33}$ superstructure and the anti-Fe_2P-type structure (upper left), and between the superstructure and the fluorite-type structure (lower right).

The anti-Fe_2P forms prepared from precursors of different-sized *Ln* cations in BaX_2–LnX_3 precursors differ slightly (*3*). The *c* axis deviation appears significant and the precursor with the larger cation produces the anti-Fe_2P form with the smaller unit cell volume. Deviations are small, but are not due to experimental error since they are reproducible for both chlorides and bromides and are apparent visually in the X-ray powder diffraction photographs. The larger

TABLE II

COMPARISON BETWEEN THE LATTICE PARAMETERS OBSERVED FOR METASTABLE (FLUORITE-TYPE) $LnCl_2$ AND THOSE DERIVED THROUGH GEOMETRICAL RELATIONSHIPS FROM THE (HEXAGONAL) a_h AND c_h LATTICE PARAMETERS OF THE $Ln_{14}Cl_{33}$ PRECURSORS

Precursor $Ln_{14}Cl_{33}$	Precursor parameters	$LnCl_2$ parameter	
		Derived	Observed
Ln = Sm	a_h 12.864(2) Å	6.87 Å	6.9827(5) Å
	c_h 24.72(8)	7.14	6.9827(5)
Ln = Eu	a_h 12.815(4)	6.85	6.961(1)
	c_h 24.768(8)	7.15	6.961(1)

Note. Derived $a_{cubic} = 0.534 \cdot a_h$ and $a_{cubic} = 0.2887 \cdot c_h$. See text.

TABLE III

RELATIONSHIP BETWEEN THE MX_2 METASTABLE STRUCTURE-TYPE PRODUCED BY SOLVOLYTIC DECOMPOSITION AND THE X^-/M^{2+} AND M^{2+}/Ln^{3+} IONIC RADII

Precursor system	Radius ratio		MX_2 structure type
	X^-/M^{2+}	M^{2+}/Ln^{3+}	
$SmCl_2$–$SmCl_3$	1.18	1.16	Fluorite
$EuCl_2$–$EuCl_3$	1.20	1.14	Fluorite
$BaBr_2$–$NdBr_3$	1.17	1.28	Anti-Fe_2P
$BaCl_2$–$SmCl_3$	1.07	1.28	Anti-Fe_2P

TABLE IV

COMPARISON BETWEEN THE LATTICE PARAMETERS OBSERVED FOR METASTABLE (ANTI-Fe_2P-TYPE) $BaBr_2$ AND THOSE DERIVED THROUGH GEOMETRICAL RELATIONSHIPS FROM THE (HEXAGONAL) a_h AND c_h LATTICE PARAMETERS OF THE $Ba_9Ln_5Br_{33}$ PRECURSORS

Precursor		Precursor parameters	$BaBr_2$ parameters	
			Derived	Observed
$Ba_9Nd_5Br_{33}$	a_h	14.039(1) Å	9.17 Å	8.4814(8) Å
	c_h	26.477(4)	4.41	4.8393(7)
$Ba_9La_5Br_{33}$	a_h	14.098(2)	9.21	8.4826(6)
	c_h	26.678(6)	4.45	4.824(1)

Note. Derived $a_h(BaX_2) = 0.653 \cdot a_h$(precursor) and $c_h(BaX_2) = c_h$(precursor)/6. See text.

La^{3+} cation apparently creates higher "internal pressure" than do the smaller Nd^{3+} and Sm^{3+} cations.

Again, from the apparent cell geometry we can establish the relationship between the two sets of lattice parameters as $a_h(BaX_2)/a_h(\text{super}) = 0.653$, or $a_h(BaX_2) = 0.653 \cdot a_h(\text{super})$, and $c_h(BaX_2) = c_h(\text{super})/6$. Derived and observed parameters are compared in Table IV; note the much larger deviation between derived and observed parameters in this case than in the fluorite case (Table II). To form the anti-Fe_2P-type structure the cations must undergo significant in-layer reorganization and out-of-layer displacement. This can be understood by comparing Figs. 3a and 3c. As a result of the displacement the a_h axis (in-layer) shortens substantially while the c_h axis elongates. The slower rate of formation of the anti-Fe_2P-type structure in comparison to that of the fluorite-type structure can now be understood. The former reaction involves a three-dimensional change while the latter is nearly two dimensional and should have a lower activation energy.

It is indeed unusual that the solvolytic decomposition product of $Ba_9Ln_5Br_{33}$ is anti-Fe_2P-type and not $PbCl_2$-type $BaBr_2$ since the latter is the thermodynamically more stable modification and has a layer structure and coordination polyhedra similar to those of the anti-Fe_2P-type structure (*13*). The principal difference between the two structure types lies in their symmetries. The anti-Fe_2P-type structure has higher symmetry than does the $PbCl_2$-type. In fact, the highest symmetry element in the anti-Fe_2P-type structure, the six-fold inversion axis, is created when the threefold inversion axis in the precursor is destroyed. Therefore, low-temperature solvolytic decompositions of mixed halides must be both topochemically and symmetry controlled.

Acknowledgments

Support of the National Science Foundation, Division of Materials Research, Solid State Chemistry Program DMR 84-00739, and the Michigan State University Center for Fundamental Materials Research is acknowledged gratefully.

References

1. A. F. CLIFFORD AND K. J. HUGHES, *in* "Rare Earth Research III" (L. Eyring, Ed.), p. 677–686, and references therein, Gordon and Breach, New York (1965).
2. G. LIU AND H. A. EICK, *Inorg. Chem.* **27,** 2161 (1988).
3. G. LIU AND H. A. EICK, *J. Less-Common Metals* **149,** 47 (1989).
4. P. E. WERNER, L. ERIKSSON, AND M. WESTDAHL, *J. Appl. Crystallogr.* **18,** 367 (1985).
5. P. M. DE WOLFF, *J. Appl. Crystallogr.* **1,** 108 (1968).
6. D. A. JOHNSON, *in* "Some Thermodynamic Aspects of Inorganic Chemistry," 2nd ed., p. 30 ff. Cambridge University Press, New York (1982).
7. U. LÖCHNER, Ph.D. dissertation, Universität Karlsruhe (1980).
8. A. HAASE AND G. BRAUER, *Z. Anorg. Allg. Chem.* **441,** 181 (1978).
9. R. GIOVANOLI, W. FEITKNECHT, R. MAURER, AND H. HAENI, *Chimia* **30,** 307 (1976).
10. K. ROSSMANITH, *Monatsh. Chem.* **110,** 109 (1979).
11. Z. C. KANG, L. MACHESKY, H. A. EICK, AND L. EYRING, *J. Solid State Chem.* **75,** 73 (1988).
12. H. BÄRNIGHAUSEN, *Rev. Chim. Miner.* **10,** 77 (1973).
13. H. P. BECK, *J. Solid State Chem.* **47,** 328 (1983).
14. M. EITEL, Ph.D. dissertation, Universität Karlsruhe (1985).

15. S. E. NESS, D. J. M. BEVAN, AND H. J. ROSSELL, *Eur. J. Solid State Inorg. Chem.* **25,** 509 (1988).
16. D. J. M. BEVAN, J. STRÄHLE, AND O. GREIS, *J. Solid State Chem.* **44,** 75 (1982).
17. G. LIU AND H. A. EICK, unpublished results.
18. Powder Diffraction File, JCPDS: International Centre for Diffraction Data, 1601 Park Lane, Swarthmore, PA 19081, File No. 24–95.
19. R. D. SHANNON, *Acta Crystallogr. Sect A* **32,** 751 (1976).